Int. J. Heat Mass Transfer. Vol. 36, No. 2, pp. 337–345, 1993
Printed in Great Britain

0017–9310/93 $6.00 + 0.00

Instantaneous local heat transfer coefficients and related frequency spectra for a horizontal cylinder in a high temperature fluidized bed

A. H. GEORGE
Department of Mechanical Engineering, Montana State University, Bozeman, MT 59717, U.S.A.

(*Received* 5 *November* 1991 *and in final form* 27 *February* 1992)

Abstract—Experimental data are reported for instantaneous local heat transfer coefficients on the surface of an immersed 50.8 mm diameter horizontal cylinder in a high temperature (562°C) fluidized bed of particles with 1 mm mean size using air as the fluidizing gas. Comparison of the reported data with analytical models of bed-to-surface heat transfer shows good agreement for heat transfer near particle contact points and in the interstitial channels between particles. The shallow bed height above the instrumented cylinder (0.10 m) allowed bubbles to erupt to the surface while still in contact with the cylinder. Heat transfer during periods of bubble phase contact increased, compared to the case of fully immersed bubbles, by a factor of 2 or 3 due to erupting bubbles contacting the cylinder. The frequency spectra related to the instantaneous local heat transfer coefficients displayed sharp maxima at low frequencies (0.36–1.46 Hz). Based on these frequency spectra, it is suggested that instrumentation for similar measurements be designed for a bandwidth of at least 100 Hz.

INTRODUCTION

FLUIDIZED bed heat transfer studies that are conducted exclusively at low (ambient) temperature have several important limitations. The most serious limitation is that the transport properties of the fluidizing gas and particles are essentially fixed and will usually have values greatly different than characteristic of high temperature operation. Radiant heat exchange, which is not negligible in fluidized bed combustors or other high temperature fluidized beds, cannot be studied under low temperature conditions. Validation of analytical models or empirical data correlations for bed-to-surface heat transfer based exclusively on studies conducted in low temperature fluidized beds is, therefore, not conclusive. The geometry, i.e. the immersed horizontal cylinder, considered in this work is of importance since many fluidized bed combustors use arrays of immersed horizontal tubes as heat transfer surfaces [1].

Instantaneous local heat transfer coefficient measurements establish both the bubble phase and the emulsion phase contributions to the local heat transfer coefficient. Via Fourier analysis, the frequency spectra corresponding to the instantaneous local heat transfer coefficients can be computed. These frequency spectra are useful in the design of instruments to measure instantaneous local surface temperature or instantaneous local heat transfer coefficients. The measurement system must respond accurately to inputs at all frequencies that are significantly present. Therefore, the frequency spectra related to the instantaneous local heat transfer coefficients are of considerable value.

Few measurements of instantaneous local heat transfer coefficients for surfaces immersed in fluidized beds at elevated temperature have been reported. Instrumentation for making this specific measurement was developed and tested previously [2] and later adapted to horizontal tubes [3]. With few modifications, the instrumentation developed in the latter work was used in the present work.

The measurement of time-averaged local heat transfer coefficients does not require a rapidly responding heat flux transducer and is therefore easier to perform than instantaneous measurements. Time-averaged local heat fluxes (or, equivalently, time-averaged local heat transfer coefficients) for horizontal tubes immersed in high temperature fluidized beds have been reported by a few investigators [4–6]. While these data provide useful information concerning the local heat transfer coefficient around the periphery of an immersed tube, no information whatsoever is provided concerning the temporal variation of the local heat transfer coefficient. The more detailed models of the heat transfer process, including those used as a basis for comparison with the experimental data presented below, involve the calculation of instantaneous bed-to-surface heat transfer rates from the instantaneous flow field and voidage distribution near the immersed surface. Time-averaged data are not adequate for validation or improvement of these analytical models.

Significant improvements in both the instrumentation and the fluidized bed combined to make the data reported below more reliable than reported previously [3]. Therefore, a more detailed analysis of the data including comparison of the instantaneous

NOMENCLATURE

d_p	mean particle size
h	instantaneous local heat transfer coefficient
h_B	instantaneous local heat transfer coefficient during bubble phase contact
$\langle h \rangle$	time-averaged local heat transfer coefficient
Nu_{p2D}	Nusselt number for the interstitial channel based on particle diameter and properties at the fluidized bed temperature
Pr	Prandtl number
q_w	instantaneous local bed-to-surface heat flux
r_p	mean particle radius
Re_c	Reynolds number for the interstitial channel based on local interstitial gas velocity, particle diameter and properties at the fluidized bed temperature
s_p	one-half of the center-to-center particle spacing
t	time
T_{bed}	fluidized bed temperature
T_w	surface temperature
$\langle T_w \rangle$	time-averaged local surface temperature
u'	turbulence intensity
U_0	superficial gas velocity
U_{mf}	superficial gas velocity at minimum fluidization
V_B	average vertical gas velocity in bubble based on maximum flow area.

Greek symbols

θ	angular positions on cylinder referred to 0° at the bottom of the cylinder.

Subscripts

B	bubble phase
bed	fluidized bed
c	interstitial channel
2D	two-dimensional boundary layer
mf	minimum fluidization
p	particle
w	surface of immersed cylinder.

local heat transfer coefficients with applicable analytical models, calculation of the frequency spectra of the instantaneous local heat transfer coefficients, and calculation of the time fraction of local bubble contact was performed.

An excellent recent (1989) review (236 references) of fluidized bed heat transfer including experimental data, analytical models and instrumentation is given by Saxena [7]. No experimental data for instantaneous local heat transfer coefficients to immersed objects in fluidized beds at elevated temperature or associated instrumentation are, however, reported in the cited work. Lack of such data motivated the study reported below.

EQUIPMENT

Instrumentation

The major items of instrumentation used in the present study were: (1) the 50.8 mm diameter instrumented cylinder with heat flux transducer for measuring the instantaneous local heat flux, (2) the signal conditioning circuit which provides a voltage output that is linearly related to the instantaneous local heat flux, (3) the reference heat flux transducers used for calibration and (4) the digital data acquisition system. Since all of these items have been described in a previous paper [3] only those modifications that are relevant to the current work will be further described.

Figure 1, which shows the heat flux transducer and the active portion of the heat flux transducer mounted in the cylinder wall, is provided for immediate reference. As shown, the active portion of the heat flux transducer was contoured to match the outer surface of the cylinder. Both the instrumented cylinder and

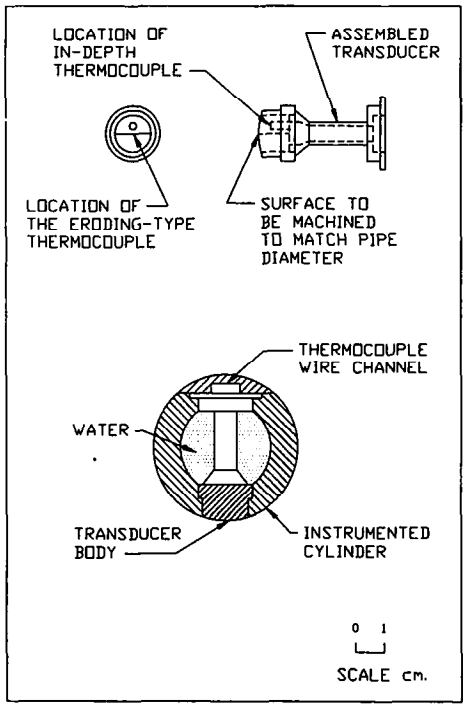

FIG. 1. Heat flux transducer and active portion of the heat flux transducer mounted in the cylinder wall.

the heat flux transducer were constructed of type 304 stainless steel. The transducer was nonintrusive and did not significantly disturb the flow of gas and particles around the cylinder or the thermal boundary layer at the surface of the cylinder.

Measurement of the instantaneous local surface temperature and the in-depth temperature (about 6 mm from the surface in this design) was required to solve the conduction problem for the transducer body and, subsequently, computation of the instantaneous local heat flux at the surface. The surface temperature was measured by an eroding thermocouple junction [2, 3] while the in-depth temperature was measured by a welded thermocouple junction of conventional design. The two temperature measuring elements in the heat flux transducer were constructed of ANSI type E thermocouple wire rather than the ANSI type K thermocouple wire used previously. This change of thermocouple wire type provided an increase in thermocouple voltage output of approximately 60% and helped to improve the signal-to-noise ratio of the instantaneous local heat flux measurements.

The instrumented cylinder was water-cooled with coolant supplied through rotary unions. This mounting arrangement allowed rotation of the cylinder to different angular positions without disconnecting any piping. A single heat flux transducer was used for all of the instantaneous local heat flux measurements reported in this work.

A new signal conditioning circuit, of essentially the same design as used previously [3], was built with great attention given to component quality, grounding and shielding. As before, the signal conditioning circuit provided an output voltage which was linearly related to the instantaneous local heat flux on the surface of the cylinder. The new circuit provided a noise output of 20 mV peak-to-peak which, for the conditions of operation reported below, corresponds to a fluctuation in the measured instantaneous local heat transfer coefficient of approximately 9 W m^{-2} K^{-1} peak-to-peak. In the earlier work [3], the comparable figure was 44 W m^{-2} K^{-1} peak-to-peak. Therefore, a significant improvement in the heat flux transducer and associated signal conditioning circuit was achieved.

The settling time (defined as the time interval after application of a step change in surface heat flux for the output voltage, which is linearly related to the surface heat flux, to remain within 2% of final value) of the combined heat flux transducer and signal conditioning circuit was 4 ms. Peak overshoot was less than 1%.

Calibration of the combined heat flux transducer and signal conditioning circuit was performed as in the earlier work [3]. Specification of uncertainty in heat flux measurements is difficult. However, based on the accuracy of the reference transducers used in the calibration procedure and the repeatability of the calibration results, the uncertainty in the heat flux calibration was estimated to be $\pm 20\%$.

From the measured values of the instantaneous local heat flux, fluidized bed temperature and time-averaged surface temperature, the corresponding instantaneous local heat transfer coefficient was computed

$$h = \frac{q_w}{T_{bed} - \langle T_w \rangle}. \quad (1)$$

The data acquisition system was improved by using a Hewlett–Packard model 9836 computer for system control. This improvement allowed a sampling interval of 2 ms to be used rather than the 5 ms sampling interval used in the previous work [3]. The shorter sampling interval is more compatible with the settling time of the combined heat flux transducer and signal conditioning circuit. Based on the Nyquist sampling rate criteria [8], the sampling interval used in this work is adequate to determine the frequency spectra of the instantaneous local heat transfer coefficients up to a frequency of 250 Hz.

Fluidized bed

The high temperature fluidized bed with 0.30×0.60 m cross-section was described previously [3]. A new distributor plate was, however, installed to support the present work. The distributor plate was constructed of 3.2 mm thick Haynes alloy 230 with 456 holes of 6.4 mm diameter in a square array pattern with 19.1 mm center-to-center spacing. A 16 mesh type 304 stainless steel screen was placed below the distributor plate. This new distributor plate eliminated the problem of non-uniform fluidization, caused by a warped distributor plate, that influenced the results of the aforementioned study. Stability of the fluidized bed operating temperature was also improved by the new distributor plate. Propane was used as a fuel gas to heat the air under the distributor plate and, subsequently, the fluidized bed. No combustion occurred in the fluidized bed itself.

TEST CONDITIONS

The instrumented cylinder was mounted horizontally in the fluidized bed approximately 0.36 m above the distributor plate. The packed bed height was 0.10 m above the centerline of the instrumented cylinder. This rather shallow bed height above the instrumented cylinder allowed bubbles to erupt to the surface while the lower portion of the bubbles were still in contact with the cylinder. Visual observation of the fluidized bed from the top allowed the cylinder to be seen within erupting bubbles several times per minute. At the moment that the bubble erupts to the surface the pressure within the bubble equalizes to that existing in the freeboard. Therefore, the erupting bubble represents a path of very low flow resistance and vertical gas velocity in the erupting bubble will greatly exceed that in a fully immersed bubble. The classical analysis of Davidson [9] indicates that the

average vertical velocity at the central plane of a fully immersed spherical bubble is $3U_{mf}$. A recent numerical analysis of gas flow in erupting bubbles by Yule and Glicksman [10] indicates much higher values (up to approximately $50U_{mf}$) for the average vertical gas velocity within an erupting bubble.

Granular refractory material with commercial designation Ione Grain was used as bed material (particles). This material had a solids density of 2700 kg m^{-3} and a surface mean particle size [11] of 1.00 mm. The chemical composition, specific heat and thermal conductivity of the bed material, for a range of temperatures, are given in ref. [6]. The fluidized bed was operated at 562°C and 1 atm and the measured minimum fluidization velocity was 0.47 m s^{-1}. A superficial gas velocity of 1.00 m s^{-1} was used ($U_0/U_{mf} = 2.13$).

For the operating conditions outlined above, the fluidized bed operated in the slow bubble regime as defined in ref. [12]. Fairly intense bubbling but no slugging occurred during operation. The particles are in Geldart Group D [13], Group I (at a fluidized bed temperature of 562°C) or Group IIA (at room temperature) in the Saxena and Ganzha [14] classification scheme.

Test procedure

Each test sequence consisted of instantaneous local heat flux measurements being recorded at five angular positions around the immersed horizontal cylinder. Angular positions θ referred to below are referenced to the lower stagnation point of the cylinder, i.e. the 0° position corresponds to the bottom of the cylinder and the 180° position corresponds to the top of the cylinder.

The fluidized bed was allowed to reach steady state operating conditions at the selected temperature and superficial gas velocity. A data acquisition system (Hewlett–Packard HP3054A with 3456 and 3437 voltmeters and a 9836 computer) was then used to take 120 s of instantaneous local heat flux measurements, with a sampling interval of 2 ms, for each of the five angular positions. The first data set was taken at $\theta = 0°$; then the cylinder was rotated 45° and the next data set was recorded. This procedure was repeated until data were taken at all five angular positions.

The voltages required to compute the time-averaged local surface temperature were also recorded by the data acquisition system. The bed temperature was maintained within ±3°C of the specified value for all cases considered.

TEST RESULTS

Instantaneous local heat transfer coefficients

Figures 2–6 show 2 s of typical instantaneous local heat transfer coefficient values for the run conditions reported above. The time intervals have been selected to display phenomena which provide insight into the bed-to-surface heat transfer process.

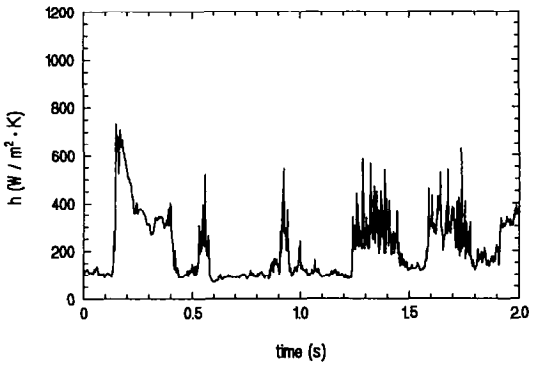

FIG. 2. Instantaneous local heat transfer coefficient for $d_p = 1.0$ mm, $\theta = 0°$, $U_0 = 1$ m s^{-1}, $T_{bed} = 562°C$.

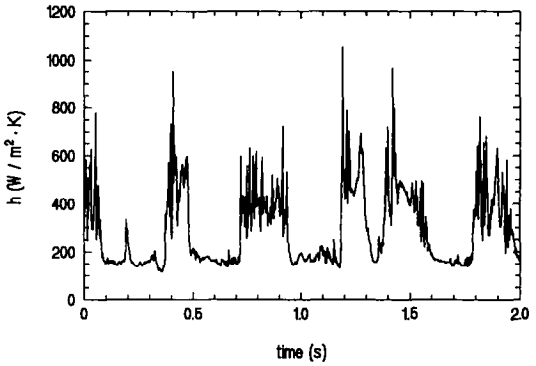

FIG. 3. Instantaneous local heat transfer coefficient for $d_p = 1.0$ mm, $\theta = 45°$, $U_0 = 1$ m s^{-1}, $T_{bed} = 562°C$.

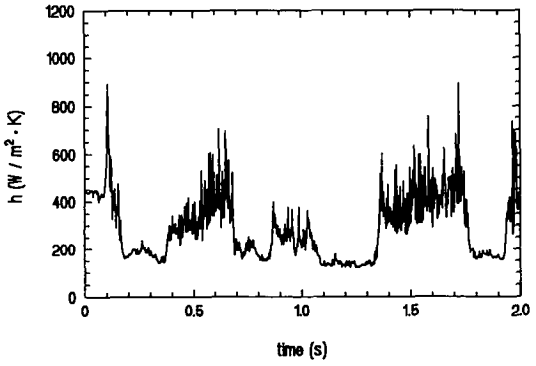

FIG. 4. Instantaneous local heat transfer coefficient for $d_p = 1.0$ mm, $\theta = 90°$, $U_0 = 1$ m s^{-1}, $T_{bed} = 562°C$.

Local contact between the fluidized bed and the surface of the cylinder can be divided, at least approximately, into three basic types: (1) bubble phase contact during which essentially pure gas contacts the surface, (2) nearly stationary emulsion phase contact during which emulsion phase is in contact with the surface but does not slide significantly with respect to the surface and (3) moving emulsion phase contact during which the emulsion phase slides with respect to the surface. For the particle size and operating conditions considered in this work, the characteristics of

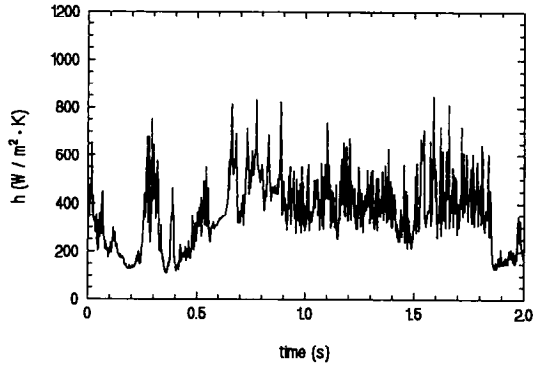

FIG. 5. Instantaneous local heat transfer coefficient for $d_p = 1.0$ mm, $\theta = 135°$, $U_0 = 1$ m s^{-1}, $T_{bed} = 562°C$.

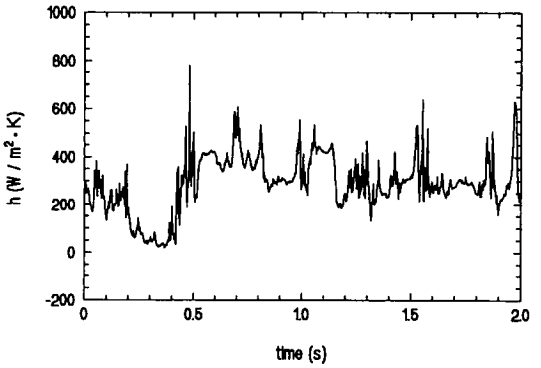

FIG. 6. Instantaneous local heat transfer coefficient for $d_p = 1.0$ mm, $\theta = 180°$, $U_0 = 1$ m s^{-1}, $T_{bed} = 562°C$.

the instantaneous local heat transfer coefficient corresponding to each type of local contact are: (1) bubble phase contact is characterized by a relatively low (with respect to the time-averaged local heat transfer coefficient) and approximately constant heat transfer coefficient, (2) nearly stationary emulsion phase contact is characterized by an initially high heat transfer coefficient followed by a decreasing heat transfer coefficient as the emulsion phase cools and (3) moving emulsion phase contact is characterized by a high heat transfer coefficient with large high frequency temporal variations. During contact of this type, the heat flux transducer is alternately subjected to direct particle contact and to contact with the gas in the interstitial channels between particles.

Values of the time-averaged local heat transfer coefficient and the time fraction of local bubble phase contact reported below are based on the entire 120 s of data taken for each angular position. Since the relative amounts of each type of contact between the fluidized bed and surface are functions of angular position, the results pertaining to each angular position are discussed separately.

Angular position 0°. The heat transfer at the lower stagnation point is characterized by relatively long time intervals of bubble contact. For example, the data shown in Fig. 2 indicate bubble contact for the time intervals 0–0.12 and 0.58–0.90 s. While direct observation of the gas bubbles contacting the tube was not possible in the high temperature fluidized bed, except for the view of erupting bubbles from the top; certainly the bubbles varied in size, shape, and the manner in which they intersected the horizontal cylinder. Therefore, it is interesting that the instantaneous local heat transfer coefficient during bubble contact has a nearly constant value of approximately 100 W m^{-2} K^{-1}. The same figure indicates nearly stationary emulsion contact for the time interval 0.13–0.30 s and moving emulsion phase contact for the intervals 1.23–1.45 and 1.60–1.76 s. The data in Fig. 2 show clear evidence of frequent emulsion phase contact. A heat transfer model based on gas convection alone would not be appropriate even at the lower stagnation point of a horizontal cylinder.

Angular position 45°. Figure 3 shows typical heat transfer data for this position. Bubble contact is evident with an instantaneous local heat transfer coefficient of approximately 140 W m^{-2} K^{-1}. Particles within the bubble or turbulence in the free stream outside the boundary layer cause larger fluctuations in the heat transfer coefficient during bubble contact than was the case at the lower stagnation point. Moving emulsion phase contact is common but stationary emulsion phase contact rarely occurs at this position.

Angular position 90°. As shown in Fig. 4, bubble contact at this position provides an instantaneous local heat transfer coefficient of approximately 140 W m^{-2} K^{-1}. Periods of moving emulsion contact are of relatively long duration, e.g. the time interval 1.35–1.75 s. During periods of moving emulsion contact, the heat transfer coefficient can be sustained at a high value or even increase during the duration of the contact, e.g. the time interval 0.40–0.66 s. This is in contrast to stationary emulsion phase contact which has its maximum value at the start of the contact and then decreases with time as the emulsion cools.

Angular position 135°. As shown in Fig. 5, bubble contact at this location is relatively rare and tends to be of short duration. Moving emulsion phase contact is commonly of long duration (up to 2 s).

Angular position 180°. The top of the horizontal immersed cylinder is usually covered by a stack of defluidized particles which are moved by passing gas bubbles [15, 16]. Although infrequent at this position, bubble contact does occur, e.g. the time interval 0.20–0.38 s shown in Fig. 6. The heat transfer coefficient during periods of bubble phase contact varies from 0 to 90 W m^{-2} K^{-1} and is, therefore, significantly lower than observed at other angular positions. At this position in particular, however, identification of bubble phase contact from the instantaneous local heat transfer coefficient data is uncertain. The latter portions of stationary emulsion phase contact of long duration (greater than approximately 1 s) would be difficult to distinguish from bubble phase contact. Moving emulsion phase contact is common but the frequency

of oscillation of the instantaneous local heat transfer coefficient is lower than observed at other angular positions. Clearly, significant particle motion occurs at this position despite the presence of a defluidized stack of particles.

Comparison with analytical models of bed-to-surface heat transfer

For the fluidized bed temperature used in this study (562°C), radiant heat transfer was not a significant fraction of the total bed-to-surface heat transfer. Therefore, only the gas convective and particle convective heat transfer mechanisms are considered in the comparisons made below.

Bubble phase contact. A very detailed analytical model of bubble phase heat transfer was developed by Adams [17]. The model was validated by comparison with data taken in fluidized beds at near room temperature. This model assumes fully immersed bubbles and provides time-averaged local values of the heat transfer coefficient during periods of bubble phase contact. For the present application, the influence of free stream turbulence on the heat transfer coefficient was predicted using the correlation developed by Kestin and Wood [18] (which is supported by the work of Hoogendoorn [19]) rather than the method suggested by Adams [17] which was developed primarily to model turbulence in interstitial channels. The free stream turbulence intensity was estimated to be 0.2 based on refs. [20, 21]. For the range of parameter values considered here, this value of the free stream turbulence intensity increased the analytically predicted heat transfer coefficient by, at maximum, 18% over that computed for purely laminar flow. A voidage of 0.40 was assumed for the emulsion phase. A comparison of the present experimental results with those given by the modified Adams model is shown in Fig. 7. All gas properties were evaluated at the bed temperature. The values of the instantaneous local heat transfer coefficient during bubble phase contact displayed in the above experimental results are approximately a factor of 2 or 3 higher than predicted by the modified Adams model, with vertical gas velocity $3U_{mf}$.

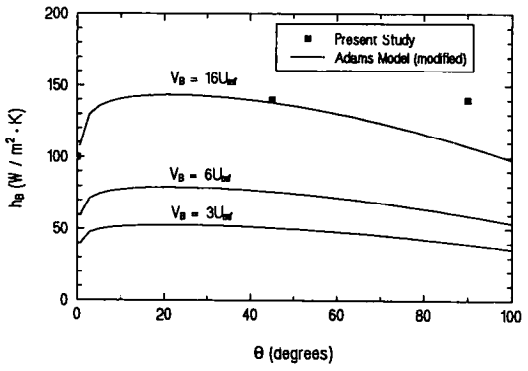

FIG. 7. Time-averaged local heat transfer coefficients during bubble phase contact compared with the values given by the modified Adams model [17] for three vertical gas velocities.

No errors in instrument calibration which could explain such a large discrepancy could be found. It is probable that the higher than analytically predicted instantaneous local heat transfer coefficients during bubble phase contact are due to the bubbles erupting to the surface rather than being fully immersed as assumed in the analytical model.

As shown by the numerical solution of Yule and Glicksman [10], the vertical gas velocity in an erupting bubble is a function of the geometry of the bubble. Their results indicate that an erupting bubble shaped like a vertical cylinder with height to diameter ratio of 2 will provide a maximum vertical gas velocity of $16U_{mf}$ while an erupting spherical bubble will provide a maximum vertical gas velocity of $6U_{mf}$. Both of these figures are much greater than the classical result by Davidson [9] which predicts a vertical velocity of $3U_{mf}$ for a fully immersed spherical bubble. Neither of these analyses include the influence of the impermeable boundary represented by the immersed cylinder. However, additional calculations were made using the modified Adams model with assumed vertical gas velocities of $6U_{mf}$ and $16U_{mf}$ rather than $3U_{mf}$ as initially assumed. The result of these calculations is shown in Fig. 7. While the agreement between the analytically predicted values of the local heat transfer coefficient and the experimental data improved by using the vertical gas velocities based on the numerical solution given in ref. [10], a fully satisfactory analytical model has not been developed for an erupting bubble in contact with an immersed cylinder.

One other recent study [22] of instantaneous local heat transfer to immersed surfaces in fluidized beds obtained a heat transfer coefficient during bubble phase contact of 110 W m^{-2} K^{-1} for a particle size of 1.2 mm and room temperature operation. This value of the heat transfer coefficient is approximately twice as high as given by the analytical model suggested in the same study which used $3U_{mf}$ as the vertical gas velocity in the bubble. It is possible that erupting bubbles in simultaneous contact with the heat transfer surface influenced the experimental results presented in ref. [22].

Emulsion phase contact: heat transfer near particle contact points. The maximum instantaneous local heat transfer coefficient that occurs during emulsion phase contact has been analyzed by several investigators [23, 24]. Usually this is called the particle convective component although unsteady conduction through the gas layer near the particle contact point is the controlling heat transfer mechanism. The latter work [24] provides, for the operating conditions considered here, a value of 14 for the instantaneous local Nusselt number based on particle diameter and with the thermal conductivity evaluated at the average of bed temperature and surface temperature. Values of the instantaneous local Nusselt number in the range of 12–16 are given in ref. [23]. These are not strictly

maximum values but rather spatial averages over a small area near the particle contact point and at least a portion of the associated interstitial channel. Therefore, heat transfer rates higher than given by the above Nusselt numbers can occur near or at the point that the particle contacts the surface. A comparison of the maximum instantaneous heat transfer coefficient predicted by the above Nusselt numbers (14 and 16) with a 10 s interval of data for the $\theta = 90°$ position is shown in Fig. 8. The local maxima of the data usually fall within the predicted range. The data for the angular position $\theta = 45°$, indicate a few (about two or three per 10 s interval) maxima up to approximately 1250 W m^{-2} K^{-1}. However, other angular positions produced maxima of about the magnitude shown in Fig. 8.

Emulsion phase contact: heat transfer in interstitial channels. The Adams [24, 25] model of bed-to-surface heat transfer assumes that the central portion of the interstitial channel between particles is covered by a 2-dimensional boundary layer and that the gas flow in the channel is stagnation-like. The cited references provide the following equation for heat transfer in the 2-dimensional boundary layer:

$$Nu_{p2D} = 0.798 Pr^{0.4} Re_c^{0.5} \times [(s_p/r_p)(0.2+0.8\exp(-0.0849u' Re_c^{0.5}))]^{-0.5} \quad (2)$$

where Re_c is the Reynolds number based on local interstitial gas velocity and particle diameter. If it is assumed that no bubbles are close enough to the immersed cylinder to influence the interstitial gas flow, the interstitial gas velocity can be estimated as $10U_{mf}$ at the $\theta = 90°$ position based on the analysis given in ref. [25]. With fluid properties based on the bed temperature and $s_p/r_p = 1.0$, the resulting estimate of the heat transfer coefficient is 222 W m^{-2} K^{-1}. A comparison of this estimate with local minima of the measured instantaneous local heat transfer coefficient during sliding emulsion phase contact at the $\theta = 90°$ position is shown in Fig. 9. The reasonable agreement between the analytically estimated and experimentally measured minima partially validates the boundary layer model used and provides at least limited confidence in the ability of the measurement system used to measure heat transfer coefficients with a spatial resolution of less than one particle diameter (1 mm in the present study).

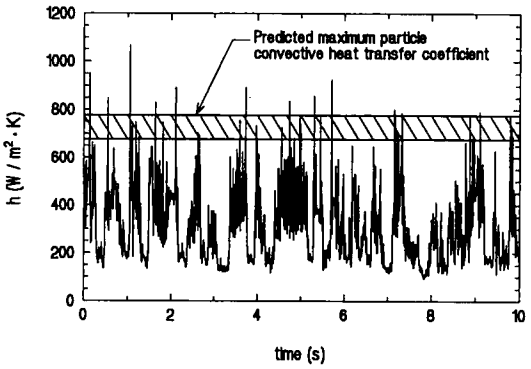

FIG. 8. Predicted maximum particle convective heat transfer coefficient [23, 24] compared with experimental data, $d_p = 1.0$ mm, $\theta = 90°$, $U_0 = 1$ m s^{-1}, $T_{bed} = 562°C$.

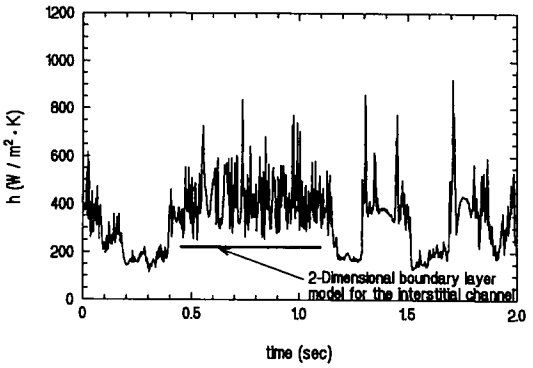

FIG. 9. Predicted minimum instantaneous local heat transfer coefficient for the interstitial channel [24, 25] compared with experimental data during moving emulsion phase contact, $d_p = 1.0$ mm, $\theta = 90°$, $U_0 = 1$ m s^{-1}, $T_{bed} = 562°C$.

Time-averaged quantities

The time-averaged local heat transfer coefficient $\langle h \rangle$, time-averaged local surface temperature $\langle T_w \rangle$, and time fraction of local bubble contact are given in Table 1. The spatially-averaged values indicated were computed from the corresponding local values using the trapezoidal rule for numerical quadrature.

The time-averaged local heat transfer coefficient values are very similar to those obtained in the earlier study [3] which used a slightly smaller particle diameter (0.9 mm) and a different distributor plate as mentioned above. The spatially-averaged heat transfer coefficient is within 2% of that obtained previously [3] and, as shown in the same work, is in very good agreement with established correlations [26–28] for the maximum spatially-averaged heat transfer coefficient. This good agreement between the measured spatially-averaged heat transfer coefficient and correlations indicates that calibration of the heat flux transducer and associated signal conditioning circuit was not seriously in error.

The time fraction of bubble contact decreases from 40% at the bottom of the cylinder to 8% at the top

Table 1. Time-averaged local heat transfer coefficient, surface temperature and time fraction of bubble contact for a horizontal cylinder in high temperature fluidized bed. $T_{bed} = 562°C$, $d_p = 1.0$ mm, $U_0 = 1.00$ m s^{-1}, $U_{mf} = 0.47$ m s^{-1}, $U_0/U_{mf} = 2.13$

	Angular position (deg)					
	0	45	90	135	180	Spatially averaged
$\langle h \rangle$ (W m^{-2} K^{-1})	219	289	322	379	318	315
$\langle T_w \rangle$ (°C)	130	136	147	167	181	151
Time fraction bubble contact (%)	40	23	14	7	8	17

of the cylinder. Since the time fraction of bubble contact is essentially the same at the angular positions 135° and 180°, it is probable that bubble contact occurs at these positions only when a large bubble surrounds the entire periphery of the cylinder. This explanation is consistent with the analytical model of bubble phase heat transfer proposed by Adams [17] which indicates that the leading edge of an attached bubble would collapse at an angular position of approximately 103°. Observations of interactions between an immersed horizontal cylinder, bubbles, and emulsion phase performed by Hagar and Thomson [29] also support this explanation.

Frequency spectra

Frequency spectra corresponding to the instantaneous local heat transfer coefficients reported were computed using a fast Fourier transform (FFT) program (Hewlett-Packard DACQ/300 Data Acquisition Manager). Space prohibits display of the frequency spectra for all cases, but the amplitude of the Fourier transform $H(\omega)$ as a function of frequency for the angular position $\theta = 0°$ is shown in Fig. 10. The figure shows that the amplitude $H(\omega)$ reaches a sharp maximum at a frequency of 1.46 Hz (accurately obtained by reading the data file from which the graph was constructed) and then decreases almost monotonically at higher frequencies. Beyond 100 Hz the amplitude $H(\omega)$ continues to decrease reaching a value of approximately 0.2 J m^{-2} K^{-1} at 250 Hz. The frequency spectra for the other angular positions had similar characteristics. For the angular positions 45°, 90° and 135°, the maximum values for $H(\omega)$ occurred at 1.40, 0.73, and 0.36 Hz, respectively. The maximum value of $H(\omega)$ for the angular position 180° was at 0.79 Hz but the maximum was less distinct than for the other cases considered and a second local maximum, of almost equal magnitude, was present at 0.40 Hz.

The frequency spectra suggest that a system for measuring instantaneous local heat transfer coefficients to objects immersed in fluidized beds, for the operating condition considered in this study, should respond accurately to surface heat flux fluctuations as rapid as 100 Hz. A significant amount of the detail in the measured quantity, i.e. the local maxima and local minima of the instantaneous local heat transfer coefficient, will be lost if a measuring system with narrower bandwidth is employed.

None of the frequency spectra displayed a significant local maximum at 60 Hz (the standard frequency for electric power distribution in the U.S.A.). This indicates that the signal conditioning circuit used to compute the instantaneous local heat flux successfully suppressed this potential noise component.

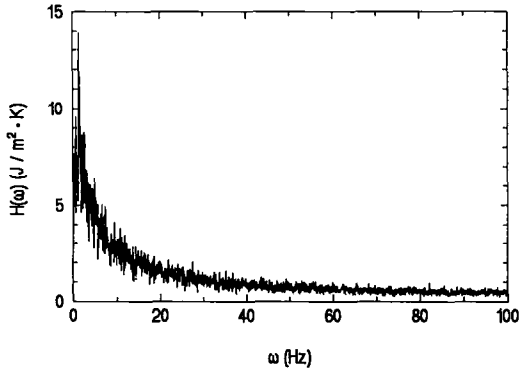

FIG. 10. Amplitude of the Fourier transform related to the instantaneous local heat transfer coefficient, $d_p = 1.0$ mm, $\theta = 0°$, $U_0 = 1$ m s^{-1}, $T_{bed} = 562°C$.

CONCLUSIONS

The main weaknesses of the present work are the limited range of operating conditions considered and the fairly high uncertainty (±20%) in the calibration of the instrument for instantaneous local heat flux measurement. Several significant conclusions can, however, be made from the unique data set presented above which provide insight into the mechanisms of fluidized bed-to-surface heat transfer and the validity of current detailed analytical models of the heat transfer process.

(1) To a good approximation, contact between the fluidized bed and the immersed surface can be divided into three types: bubble phase contact, nearly stationary emulsion phase contact and moving emulsion phase contact.

(2) The instantaneous local heat transfer coefficient data identify the type of bed-to-surface contact and allow separate measurement of instantaneous local heat transfer coefficients due to bubble contact, near particle contact points and in the interstitial channels between particles.

(3) Current models of bed-to-surface heat transfer [23–25] predicted the instantaneous local heat transfer coefficient near points of particle contact and in the interstitial channels between particles with good accuracy. Direct verification of these models under high temperature conditions has been provided.

(4) The shallow bed height above the instrumented cylinder allowed bubbles to erupt to the bed surface while still in contact with the cylinder. This operating condition caused the instantaneous local heat transfer coefficient during periods of bubble phase contact to be two or three times as high as predicted by current analytical models based on fully immersed bubbles. Reasonable agreement between analytically predicted and experimental results was achieved by using the numerical solution of ref. [10] to estimate the average vertical gas velocity in the erupting bubble. No adequate model for heat transfer to an object in contact with an erupting bubble currently exists.

(5) At least for the operating conditions considered in this work, it is suggested that instrumentation used to measure the instantaneous local heat flux have a

bandwidth of, at minimum, 100 Hz. A heat flux transducer with active area large enough to cover several particle contact points would require a smaller bandwidth since measurement of the high frequency fluctuations which occur during moving emulsion phase contact would not be possible with such a transducer.

Acknowledgements—The author wishes to thank Mr Pat Vowell for fabricating the instrumented cylinder used to take the instantaneous local heat flux data reported above and Mr John Rompel for constructing and assisting with the design of the signal conditioning circuit that was essential to the reported work. Dr J. R. Welty of Oregon State University allowed use of that institution's high temperature fluidized bed facility. Mr David Pidwerbecki assisted with the fluidized bed operation and data taking. Data processing, including graphics, was performed by Mr Carl Fehres, Mr Robert Mueller and Miss Barbara Baxter. This work was supported, in part, by the National Science Foundation (grant number CBT-8801618).

REFERENCES

1. J. Makansi and R. Schwieger, Fluidized bed boilers, *Power* **131**, S1–S15 (1987).
2. A. H. George, A transducer for the measurement of instantaneous local heat flux to surfaces immersed in high temperature fluidized beds, *Int. J. Heat Mass Transfer* **30**, 763–769 (1987).
3. A. H. George and J. L. Smalley, An instrumented cylinder for the measurement of instantaneous local heat flux in high temperature fluidized beds, *Int. J. Heat Mass Transfer* **34**, 3025–3036 (1991).
4. A. H. George and J. R. Welty, Local heat transfer coefficients for a horizontal tube in a large-particle fluidized bed at elevated temperature, *A.I.Ch.E. Jl* **30**, 482–485 (1984).
5. A. Goshayeshi, J. R. Welty, R. L. Adams and N. Alavizadeh, An experimental study of heat transfer in an array of horizontal tubes in large particle fluidized beds at elevated temperatures, 23rd ASME/AIChE Natn. Heat Transfer Conf., Denver, Colorado, U.S.A., 4–7 August (1985).
6. T. Chung and J. R. Welty, Tube array heat transfer in fluidized beds: a study of particle size effects, *A.I.Ch.E. Jl* **35**, 1170–1176 (1989).
7. S. C. Saxena, Heat transfer between immersed surfaces and gas-fluidized beds, *Adv. Heat Transfer* **19**, 97–190 (1989).
8. R. W. Hamming, *Numerical Methods for Scientists and Engineers*, 2nd Edn, p. 551. McGraw-Hill, New York (1973).
9. J. F. Davidson, Symposium on fluidization—discussion, *Trans. Inst. Chem. Engrs* **39**, 230–232 (1961).
10. T. W. Yule and L. R. Glicksman, Gas flow through erupting bubbles in fluidized beds, *A.I.Ch.E. Symp. Ser.* **84**(262), 1–9 (1988).
11. D. Kunii and O. Levenspiel, *Fluidization Engineering*, pp. 67–69. Wiley, New York (1969).
12. N. M. Catipovic, G. N. Jovanovic and T. J. Fitzgerald, Regimes of fluidization for large particles, *A.I.Ch.E. Jl* **24**, 543–546 (1978).
13. D. Geldart, Types of gas fluidization, *Powder Technol.* **7**, 285–292 (1973).
14. S. C. Saxena and V. L. Ganzha, Heat transfer to immersed surfaces in gas-fluidized beds of large particles and powder characterization, *Powder Technol.* **39**, 199–208 (1984).
15. D. H. Glass and D. Harrison, Flow patterns near a solid obstacle in a fluidized bed, *Chem. Engng Sci.* **19**, 1001–1002 (1969).
16. O. Loew, B. Schmutter and W. Resnick, Particle and bubble behavior and velocities in a large particle fluidized bed with immersed obstacles, *Powder Technol.* **22**, 45–48 (1979).
17. R. L. Adams, An approximate model of bubble phase convective heat transfer to a horizontal tube in a large particle fluidized bed, *ASME J. Heat Transfer* **104**, 565–567 (1982).
18. J. Kestin and R. T. Wood, The influence of turbulence on mass transfer from cylinders, *ASME J. Heat Transfer* **93**, 321–322 (1971).
19. C. J. Hoogendoorn, The effect of turbulence on heat transfer at a stagnation point, *Int. J. Heat Mass Transfer* **20**, 1333–1338 (1977).
20. R. L. Adams, Heat transfer in large particle bubbling fluidized beds, *ASME J. Heat Transfer* **106**, 85–90 (1984).
21. T. R. Galloway and H. Sage, A model of the mechanism of transport in packed, distended and fluidized beds, *Chem. Engng Sci.* **25**, 495–516 (1970).
22. J. Lu and R. Qian, A modelling study of the heat transfer between immersed surfaces and large-particle fluidized beds, *Int. J. Heat Mass Transfer* **32**, 2375–2384 (1989).
23. N. A. Decker and L. R. Glicksman, Conduction heat transfer at the surface of bodies immersed in gas fluidized beds of spherical particles, *A.I.Ch.E Symp. Ser.* **77**(298), 341–349 (1981).
24. R. L. Adams, Coupled gas convection and unsteady conduction effects in fluid bed heat transfer based on the single particle model, *Int. J. Heat Mass Transfer* **25**, 1819–1828 (1982).
25. R. L. Adams, An analytical model of heat transfer to a horizontal cylinder immersed in a gas-fluidized bed, Ph.D. Thesis, Oregon State University, Corvallis, Oregon, U.S.A. (1977).
26. A. P. Baskakov, B. V. Berg, O. K. Vitt, N. F. Filippovsky, V. A. Kirakosyan, J. M. Goldobin and V. K. Majkaev, Heat transfer to objects immersed in fluidized beds, *Powder Technol.* **8**, 273–282 (1973).
27. N. N. Varygin and I. G. Martyushin, Calculation of heat exchange in fluidized beds, *Khim. Mashinotr.* **5**, 6–15 (1959).
28. S. S. Zabrodsky, N. V. Antonishin and A. L. Paranas, On fluidized bed-to-surface heat transfer, *Can. J. Chem. Engng* **54**, 52–60 (1976).
29. W. R. Hager and W. J. Thomson, Bubble behavior around immersed tubes in a fluidized bed, *A.I.Ch.E. Symp. Ser.* **69**(128), 68–77 (1973).